



Article

Synthesis of Two Novel Copper (II) Complexes as Potential Inhibitors of HIV-1 Protease Enzyme: Experimental and Theoretical Investigations

Meriem Hamlaoui ^{1,*}, Ikram Hamlaoui ², Maamar Damous ^{1,3} , Youghourta Belhocine ^{3,*} , Najoua Sbei ⁴, Fatima Adam Mohamed Ali ⁵, Mashaal A. Alghamdi ⁵, Sarra Talab ⁶, Seyfeddine Rahali ⁷ and Hocine Merazig ^{1,*}

¹ Unité de Recherche de Chimie de l'Environnement et Moléculaire Structurale (URCHEMS), Département de Chimie, Université Frères Mentouri de Constantine, Constantine 25000, Algeria; damousmmaamar@yahoo.fr

² Département de Pharmacie, Faculté de Médecine, Université Saleh Boubnider, Constantine 3, Constantine 25000, Algeria; ikram.hamlaoui@univ-constantine3.dz

³ Department of Process Engineering, Faculty of Technology, 20 August 1955 University of Skikda, El Hadaik Road, Skikda 21000, Algeria

⁴ Institute of Nanotechnology, Karlsruhe Institute of Technology, Eggenstein Leopoldshafen, 76344 Karlsruhe, Germany; najwasbei89@hotmail.fr

⁵ Department of Chemistry, College of Science, Imam Mohammad Ibn Saud Islamic University (IMSIU), Riyadh 11432, Saudi Arabia; famohamedali@imamu.edu.sa (F.A.M.A.); mabalghamdi@imamu.edu.sa (M.A.A.)

⁶ Department of Chemistry, College of Applied and Industrial Science, University of Bahri, P.O. Box 11111, Khartoum 1660, Sudan; stalab9@gmail.com

⁷ Department of Chemistry, College of Science and Arts, Qassim University, Ar Rass 82571, Saudi Arabia; s.rahali@qu.edu.sa

* Correspondence: hamlaoui.meriem@yahoo.fr (M.H.); y.belhocine@univ-skikda.dz (Y.B.); hmerazig@gmail.com (H.M.)



Citation: Hamlaoui, M.; Hamlaoui, I.; Damous, M.; Belhocine, Y.; Sbei, N.; Ali, F.A.M.; Alghamdi, M.A.; Talab, S.; Rahali, S.; Merazig, H. Synthesis of Two Novel Copper (II) Complexes as Potential Inhibitors of HIV-1 Protease Enzyme: Experimental and Theoretical Investigations. *Crystals* **2022**, *12*, 1066. <https://doi.org/10.3390/cryst12081066>

Academic Editor: Waldemar Maniukiewicz

Received: 29 June 2022

Accepted: 22 July 2022

Published: 30 July 2022

Publisher's Note: MDPI stays neutral with regard to jurisdictional claims in published maps and institutional affiliations.



Copyright: © 2022 by the authors. Licensee MDPI, Basel, Switzerland. This article is an open access article distributed under the terms and conditions of the Creative Commons Attribution (CC BY) license (<https://creativecommons.org/licenses/by/4.0/>).

Abstract: In this study, we report the synthesis of two new copper complexes: [Cu(C₁₁H₇O₂)(SCN)(C₁₀H₈N₂)], denoted as (C-1), and [Cu(C₁₁H₇O₂)(C₁₂H₈N₂)Cl]·H₂O, denoted as (C-2). They are based on 2,2'-bipyridine or 1,10-phenanthroline and 2-hydroxy-1-naphthaldehyde ligands. The obtained complexes were characterized by FT-IR, UV-visible spectroscopy, and single-crystal X-ray diffraction analysis. Molecular docking was employed to predict the binding mode involved in the interaction between the two synthetic copper (II) complexes and HIV-1 protease enzyme. The X-ray structural analysis revealed that the crystal structures of both complexes are mainly stabilized by several intra- and intermolecular hydrogen bonds. The fingerprint plots associated with the Hirshfeld surfaces of both complexes clearly show that H···H interactions provide the largest contributions. According to the docking results, the synthesized complexes exhibit promising features which enable them to be bound to the HIV-1 protease enzyme.

Keywords: copper (II) complex; synthesis; HIV-1 protease enzyme inhibitor; crystal structure; non-covalent interactions; Hirshfeld surface; molecular docking

1. Introduction

In recent years, there have been several reports dedicated to the development of transition metal complexes that are based on the 2-hydroxy-1-naphthaldehyde C₁₁H₈O₂ ligand [1]. Indeed, 2-hydroxy-1-naphthaldehyde ligands can be used as a starting block for the synthesis of new ligands [2,3], or as a potential chelating agent for ions; however, only a few studies were focused on the synthesis of copper (II) complexes of bidentate ligands [4,5].

Moreover, the 2,2'-bipyridine C₁₀H₈N₂ and 1,10-phenanthroline C₁₂H₈N₂ bidentate chelating ligands are widely used as complexing moieties to form stable coordination

complexes with miscellaneous transition metal ions [6]. Transition metal complexes that have these ligands are recognized in the literature as potent antibacterial and antimicrobial agents [7–9]. It was also reported that copper complexes are good candidates for the design of novel types of protease enzyme inhibitors; here, the main goal is to treat the acquired immunodeficiency syndrome (AIDS) infection induced by the human immunodeficiency virus (HIV). Since the protease of the human immunodeficiency virus is key to the replication of the virus, the enzyme is therefore considered an attractive target for antiviral therapy; thus, the treatment strategy for AIDS involves the inhibition of HIV-1 protease [10]. To date, real progress in terms of therapy for AIDS has been achieved by using peptide-based therapeutics; however, the toxicity of peptides reduces the effectiveness of this treatment [11,12]. The copper complexes, which contain non-peptide ligands that have therapeutic potential, could be an alternative methodology for the treatment of AIDS-induced diseases.

In this contribution, we describe the synthesis of two new complexes, namely, the [(2,2'-bipyridine- K^2N,N') (1-formyl-2-naphtholato- K^2O,O') (Thiocyanate-KN) copper(II)], denoted as C-1, and [(1-formyl-2-naphtholato- K^2O,O') (1,10-phenanthroline- K^2N,N') chloride copper], denoted as C-2. FT-IR, UV-visible spectroscopy, and single-crystal X-ray diffraction analysis were used to characterize and analyze the structure of the two synthesized complexes. DFT calculations using the B3LYP [13–16] functional were conducted on the molecular structures of C-1 and C-2, and the findings were compared with the X-ray crystal data. The docking of C-1 and C-2 into the HIV-1 protease active site was assessed through the calculation of binding energy with the Autodock vina program [17], and the obtained results were compared with those of the (dimethanol)bis[N-(4-methyl-2-pyridyl)-2,3,6-trimethoxybenzamide] copper (II) dimethanol diperchlorate complex as a reference (complex-ref), which was found to be a non-peptide HIV-1 protease inhibitor with an IC50 of 1.5 μ M [18]. It is well known that the most effective inhibitor is the one that forms a bond deep in the hydrophobic cavity of the HIV-1 protease active site, and is positioned in the axes of an octahedron with the four subsites S1/S2 and S'1/S'2 forming the equatorial plane. The binding pocket of this enzyme includes the Asp25 (25')-Thr26 (26')-Gly27(27) catalytic triad and flap regions, which are most likely involved in the binding process of substrates or inhibitors [19,20].

2. Experimental

2.1. Materials and Instruments

All reagents and solvents were purchased from commercial sources (Sigma-Aldrich, St. Louis, MI, USA), and they were used in the form in which they were received.

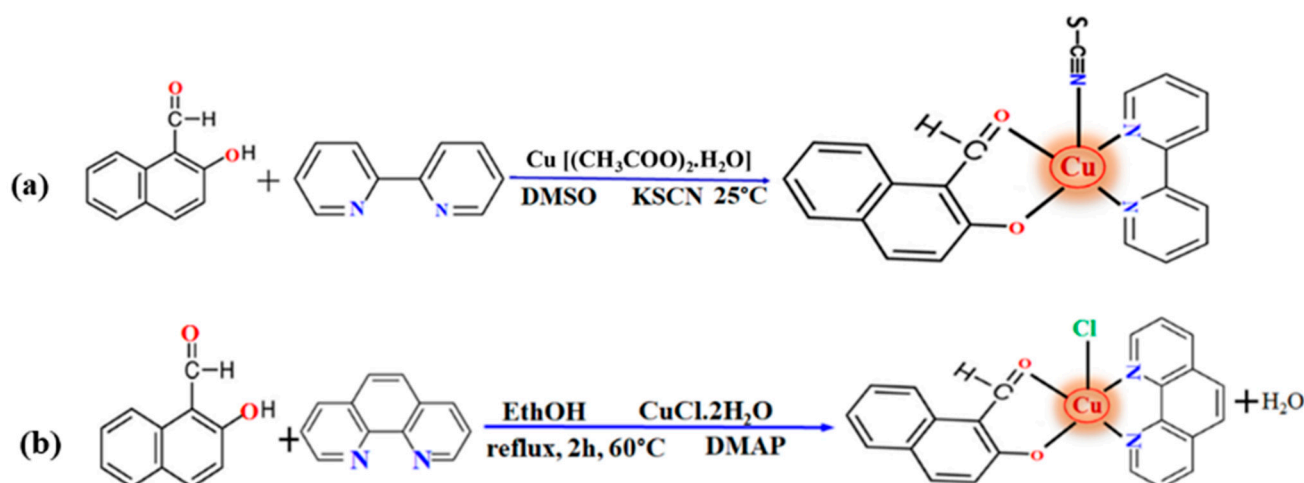
Infrared spectra were recorded in the range of 4000–400 cm^{-1} on a FT-IR Bruker ATR Vertex 70 Spectrometer. UV-visible spectra were recorded on a UV-visible Spectrophotometer Optizen 1220. The absorbance of ligands and their metals complexes were measured in DMSO in a concentration of 10^{-5} $\text{mol}\cdot\text{L}^{-1}$, in a wavelength range of 280–440 nm.

Crystals suitable for single crystal X-ray diffraction were selected, and the lattice parameters were determined using an APEXII Bruker diffractometer.

2.2. General Procedure for the Synthesis of C-1 and C-2

2.2.1. Synthesis of [(2,2'-Bipyridine- K^2N,N') (1-formyl-2-Naphtholato- K^2O,O') (Thiocyanate-KN)-Copper (II)] (C-1)

For the synthesis of C-1, $\text{Cu}(\text{CH}_3\text{COO})_2\cdot\text{H}_2\text{O}$ (0.25 mmol) and 2-hydroxy-1-naphthaldehyde (0.125 mmol) were added and stirred into a DMSO solution containing 0.25 mmol of 2,2'-bipyridine and 0.125 mmol of KSCN. The mixture was stirred for 1 h at $T = 25$ °C (Scheme 1a). After several days of slow evaporation, light green crystals appeared. This complex is stable in the air and soluble only in DMSO. Yield: 61%. IR (cm^{-1}): 2063.83(s), 1604.77(s), 1577.77(s), 1531.48(s), 1423.47(s), 1392.61(s), 1365.60(s), 1311.59(m), 1184.29(m), 1141.86(w), 1014.56(s), 972.12(w), 948.98(m), 829.39(m), 721.38(s), 636.51(w), 563.21(w), 497.63(w). UV-Vis (DMSO) (λ_{max} , nm): 290, 300 (π - π^*) 305, 315.



Scheme 1. Synthesis of (a) C-1, (b) C-2.

2.2.2. Synthesis of [(1-Formyl-2-naphtholato- $\text{K}^2\text{O}, \text{O}'$) (1,10-Phenanthroline- $\text{K}^2\text{N}, \text{N}'$) Chloride Copper] (C-2)

A mixture of $\text{CuCl}_2\cdot 2\text{H}_2\text{O}$ (0.167 mmol), 2-hydroxy-1-naphthaldehyde (0.167 mmol), 1,10-phenanthroline (0.167 mmol), and 4-dimethyl aminopyridine (0.167 mmol) was dissolved in ethanol. The solution was refluxed for 2 h at 60°C (Scheme 1b). After the slow evaporation of the solution, green single crystals were obtained and characterized by X-ray diffraction. Yield: 68%. IR (cm^{-1}): 1608.63(s), 1581.63(s), 1539.20(m), 1423.47(s), 1392.61(s); 1365.60(m), 852.54(s), 825.53(s), 752.24(m), 717.52(s), 543.93(s), 520.78(s), 493.78(s). UV-Vis (DMSO) (λ_{max} , nm): 290, 300 (π - π^*) 310, 325.

2.3. X-ray Diffraction

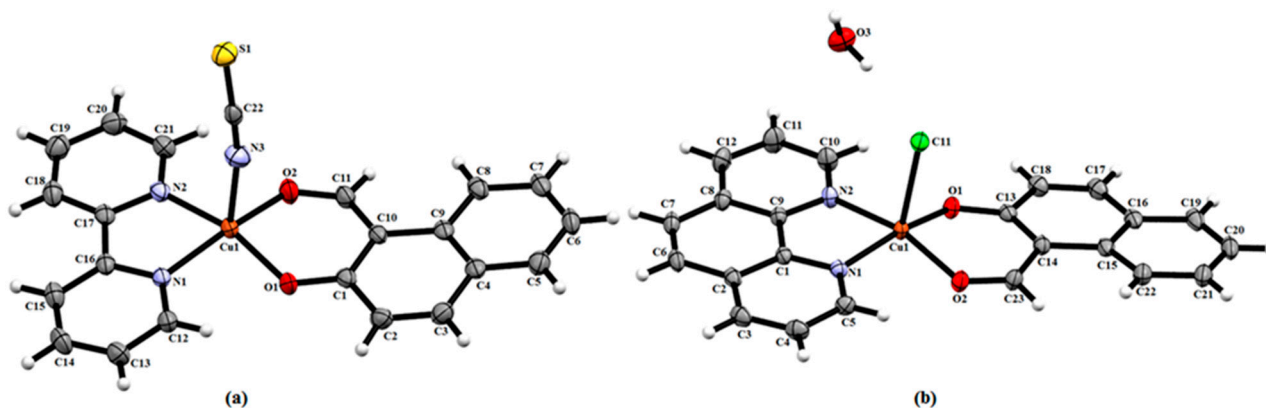
Data collection was performed using $\text{MoK}\alpha$ radiation with a BRUKER APEX2 diffractometer [21]. Cell refinement and data reduction were performed through the SAINT program. SHELXS and SHELXL [22] were used for structure solution and refinement. Structure refinement and crystal data details are reported in Table 1. All hydrogen atoms were refined in geometrically idealized positions, with $\text{C-H} = 0.93 \text{ \AA}$ for aromatic rings (2,2'-bipyridine, 1,10-phenanthroline), and they were allowed to ride on their parent atoms, with $\text{Uiso}(\text{H}) = 1.2 \text{ Ueq}(\text{C})$. The molecular structures of the two complexes are illustrated in Figure 1.

2.4. Computational Methodology

The structural optimization of C-1 and C-2 was performed using the framework of the density functional theory (DFT). The B3LYP hybrid functional was used with a 6-31 + G(d) basis set for C, H, N, Cl, O, S, and SDD for Cu. The DFT computations were conducted using the Gaussian 09W software package [23]. The PDB file of the ligand was generated using OpenBabel, version 2.4.1 [24,25]. The HIV-1 protease–ligand interaction properties were assessed by performing docking studies using AutoDock vina software. The three-dimensional structure of HIV-1 protease (PDB ID: 3TLH) was retrieved from the Protein Data Bank (<http://www.rcsb.org/pdb> (accessed on 8 March 2022)), and it was used to prepare the target site for docking calculation. The water molecules and ligand were removed from the protein, and the missing hydrogen atoms and charge were corrected. The search grid of the HIV-1 protease was identified as center_x: -6.118 , center_y: 23.382 , center_z: 36.63 with dimensions size_x: 62, size_y: 82, and size_z: 76. The best-scoring conformation was visualized and analyzed using Autodock vina tools.

Table 1. Crystallographic data and refinement parameters of C-1 and C-2.

Complex	C-1	C-2
Empirical formula	CuC ₂₂ H ₁₅ N ₃ O ₂ S	CuC ₂₃ H ₁₇ N ₂ O ₃ Cl
Formula weight	448.97	468.39
Crystal size (mm)	0.2 × 0.1 × 0.01	0.2 × 0.1 × 0.01
Temperature (K)	273	296
Crystal system	Monoclinic	Triclinic
Space group	<i>P</i> 2 ₁ / <i>n</i>	<i>P</i> -1
a (Å)	9.5832(4)	8.5321(8)
b (Å)	12.4567(5)	9.5749(9)
c (Å)	16.2129(6)	13.6821(14)
α (°)	90	93.512(5)
β (°)	102.715(2)	106.802(4)
γ (°)	90	113.281(4)
V (Å ³)	1887.95(13)	963.13(17)
Z	4	2
D _x (g cm ⁻³)	1.580	1.615
Abs. coefficient (mm ⁻¹)	1.29	1.30
Transmission factors (min, max)	0.851, 0.987	0.851, 0.987
θ Range (°)	4.4 to 27.1	4.5 to 39.4
Reflections measured	19,345	27,567
Independent reflections; R _{int}	0.068	0.0147
Reflections with I > 2σ(I)	3341	5844
Number of parameters	262	271
R(F) [I > 2σ(I)]	0.040	0.025
wR(F ²) (all data)	0.1048	0.0681
Goodness-of-fit on F ²	1.070	1.044
Δρ _{max} , Δρ _{min} (e Å ⁻³)	1.32, -0.77	0.53, -0.29

**Figure 1.** An ORTEP view of the asymmetric unit of the two complexes. (a) [Cu (C₁₁H₇O₂) (SCN) (C₁₀H₈N₂)] (C-1), (b) [Cu(C₁₁H₇O₂) (C₁₂H₈N₂) Cl]·H₂O (C-2).

3. Results and Discussions

3.1. Crystal Structure of C-1 [Cu (C₁₁H₇O₂) (SCN) (C₁₀H₈N₂)]

The single-crystal X-ray diffraction shows that the [Cu (C₁₁H₇O₂) (SCN) (C₁₀H₈N₂)] complex crystallizes in the monoclinic space group *P*2₁/*n* with *Z* = 4. The asymmetric unit of this structure is formed by a Cu(II) that coordinates with a thiocyanate ligand in an apical position, together with a nitrogen atom (N3). The coordination sphere of Cu(II) is completed by one 2,2'-bipyridine molecule acting as a bidentate ligand (through the two nitrogen atoms (N1, N2)), and one 2-hydroxy-1-naphthaldehyde (through the two oxygen atoms (O1, O2)). The Cu(II) atom has five coordinates, and it displays a square-pyramidal coordination geometry, as quantified by the value of the structural index [26] τ₅ = 0.019 (τ₅ = (β - α)/60, where β = N1-Cu1-O2 = 164.11° and α = N2-Cu1-O1 = 162.97°). (Perfect

coordination geometries of square pyramidal and trigonal bipyramidal arrangements are associated with the τ_5 values of zero and unity, respectively). The basal plane is formed by (O1, O2, N1, N2) and N3 atoms in the axial site (Figure 2a).

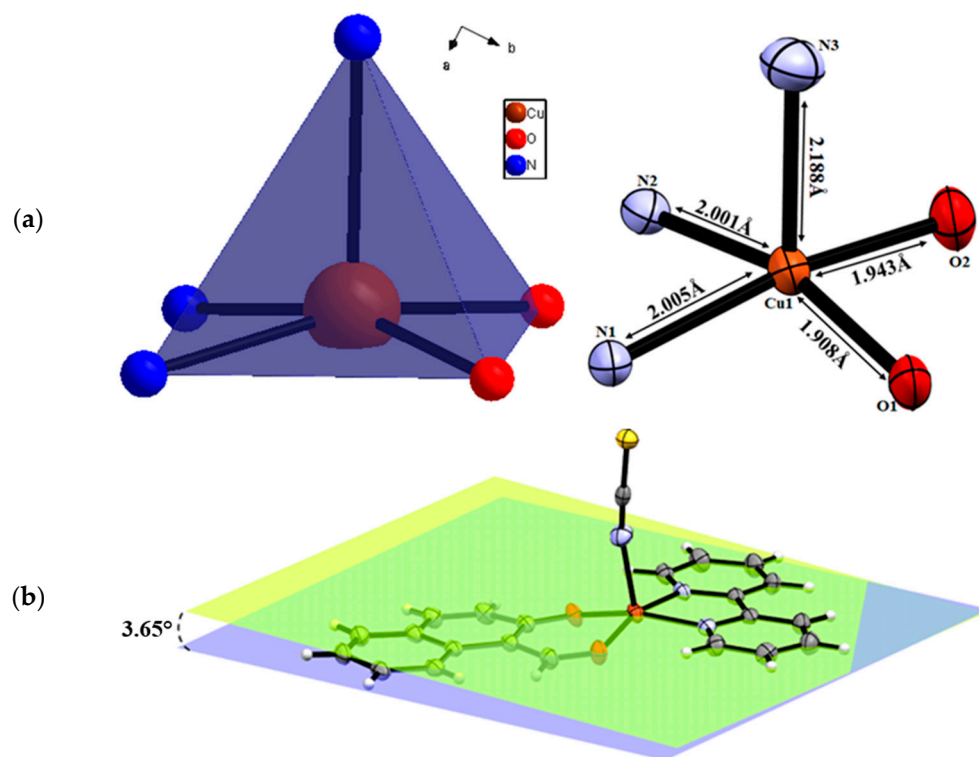


Figure 2. The copper square-pyramidal environment (a), and the dihedral angle between the two ligands (b).

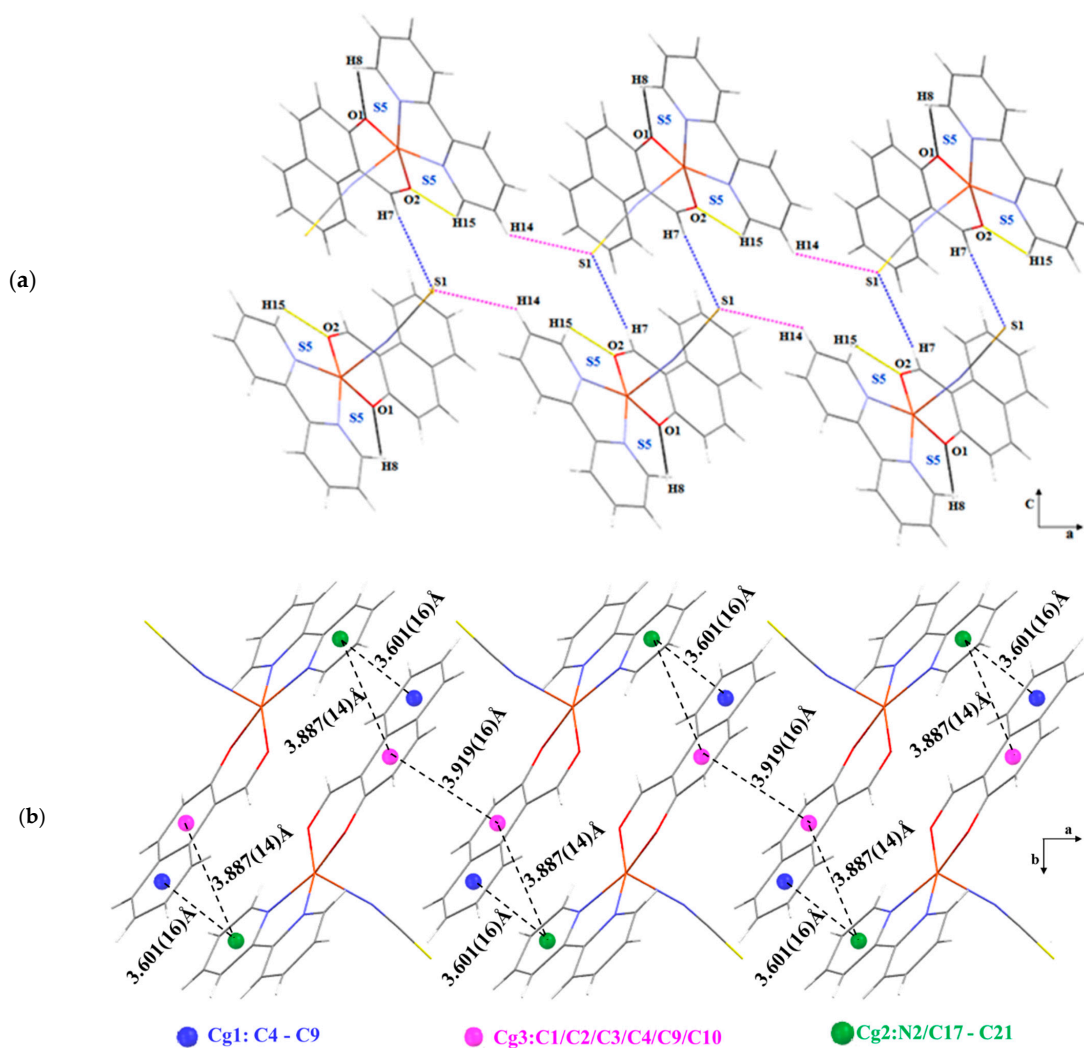
The dihedral angle between the two planes that contain ligands is 3.65° . The Cu-N and Cu-O distances in the basal plane are [(Cu1-N1 = 2.005 Å, Cu1-N2 = 2.001 Å, Cu1-O1 = 1.908 Å, Cu1-O2 = 1.943 Å], and the apical Cu1-N3 bond 2.188 Å is longer than those of the basal plane (Table S1); this is in accordance with the data in the literature [27]. These parameters were also calculated in the gas phase using the B3LYP functional, and the results indicate that the calculated bond lengths in the copper coordination sphere agree with the corresponding experimental values within a maximum deviation of 2.3% (Table S1). The bond angles exhibit a maximum deviation of 10%. This discrepancy between the experimental and theoretical values may be due to environmental effects; indeed, the theoretical values were obtained from gas-phase DFT calculations, whereas the experimental values were taken from crystallographic data.

The crystalline structure of C-1 consists of four hydrogen bond networks (Table 2). Two intermolecular hydrogen bonds are observed between H7 of C11 with S1 ($\frac{1}{2} - x, \frac{1}{2} + y, \frac{1}{2} - z$), and H14 of C20 with S1($x + 1, y, z$). Moreover, two intramolecular hydrogen bonds of the C-H \cdots O type are established between 2,2'-bipyridine and 2-hydroxy-1-naphthaldehyde, subsequently generating S(5) ring motifs [28,29]; thus, the presence of hydrogen-bond networks points to the significant role of intra and intermolecular hydrogen bonding in terms of the stabilization of complex structures. Indeed, the networks facilitate intramolecular contact and they hold the chains in a zig-zag arrangement along the a-axis (Figure 3a).

Table 2. Hydrogen-bond geometry (Å, °) in C-1 and C-2 complexes.

C-1 complex				
D-H...A	D-H	H...A	D...A	D-H...A
C11- H7...S1 ⁱ	0.93	2.84	3.729 (3)	161
C20- H14...S1 ⁱⁱ	0.93	2.97	3.621 (3)	128
C12- H8...O1	0.93	2.46	2.951(3)	113
C21-H15...O2	0.93	2.50	3.002 (3)	114
C-2 complex				
D-H...A	D-H	H...A	D...A	D-H...A
O3-H (3A)...Cl1	0.85	2.73	3.206 (14)	169
O3-H (3B)...Cl1 ^{III}	0.85	2.40	3.246 (13)	178
C3-H3...O3 ^{II}	0.93	2.54	3.436 (19)	162
C4-H4...O3 ^V	0.93	2.32	3.243 (2)	174
C5-H5...O2	0.93	2.54	3.003 (16)	111
C6-H6...Cl1 ^{II}	0.93	2.82	3.657 (15)	151
C12-H12...Cl1 ^{IV}	0.93	2.77	3.475 (18)	133
C19-H19...Cl1 ^I	0.93	2.82	3.597 (15)	142

Symmetry codes: (i) $-x + 1/2, y + 1/2, -z + 1/2$; (ii) $x + 1, y, z$; (I): $1 - x, -y, 1 - z$; (II): $-x, 1 - y, -z$; (III): $-x, -y, -z$; (IV): $-1 + x, y, z$; (V): $1 + x, 1 + y, z$.

**Figure 3.** (a) Zig-zag chains of C-1 formed by hydrogen bonds (dashed lines), (b) the aromatic ring organization with centroid-centroid distances (Å).

In addition, the C-1 complex exhibits three $\pi \cdots \pi$ stacking interactions; the first is between the centroid of the 2-hydroxy-1-naphthaldehyde ring Cg1 (C4 to C9) and the centroid of the 2,2'-bipyridine ring Cg2 (N2 and C17 to C21), with a Cg1 . . . Cg2 distance of 3.601 Å, the second is between the Cg3 (C1/C2/C3/C4/C9/C10) rings of the 2-hydroxy-1-naphthaldehyde, with a Cg3 . . . Cg3 distance of 3.919 Å, and the third is between Cg2 and Cg3, with a distance of 3.887 Å (Figure 3b).

3.2. Crystal Structure of C-2 [Cu(C₁₁H₇O₂) (C₁₂H₈N₂) Cl]·H₂O

This complex crystallizes in the triclinic system, space group *P*-1, with *Z* = 2. The asymmetric unit in this structure is composed of a copper (II) cation that is coordinated with the nitrogen atoms of the 1,10-phenanthroline, two oxygen atoms of the 2-hydroxy-1-naphthaldehyde in the equatorial plane, and a chlorine anion in the axial position. We also note the presence of a water molecule.

The Cu(II) atom adopts a square-pyramidal geometry, with a tau value of 0.02 ($\tau_5 = (\beta - \alpha)/60$, where $\beta = \text{N1-Cu1-O2} = 164.59^\circ$ and $\alpha = \text{N2-Cu1-O1} = 163.34^\circ$). In the CuN₂O₂Cl coordination sphere, the bond lengths of Cu₁-N₁ and Cu₂-N₂ are 2.012 (10) Å and 2.007(10) Å, respectively. The bond lengths of Cu₁-O₁, Cu₁-O₂, and Cu₁-Cl₁ are 1.917 Å, 1.931 Å, and 2.537 Å, respectively (Table S2). The apical bond is longer than those of the basal plane, which is in accordance with the literature [30]. These experimental parameters were compared with those calculated in the gas phase; the calculated bond lengths in the copper coordination sphere agree with the corresponding experimental values within a maximum deviation of 3.4%, whereas the bond angles exhibit a maximum deviation of 7.4% (Figure S1a). The dihedral angle between the two planes containing the ligands is 7.33° (Figure S1b).

The structure of C-2 is stabilized as a result of the occurrence of an extensive network of C-H . . . O, C-H . . . Cl and O-H . . . Cl hydrogen bonding interactions. One intramolecular hydrogen bond is observed between H5 of C5 with O2, between 1,10-phenanthroline and 2-hydroxy-1-naphthaldehyde; this generated S(5) ring motifs and seven intermolecular hydrogen bonds, as shown in Table 2 and Figure 4a. Moreover, it is worth noting that the cohesion in the crystal is also ensured by the three weak interactions between the $\pi \cdots \pi$ stacking type. The first interaction is observed between the centroid of the 1,10-phenanthroline ring (Cu1/N1/C1/C9/N2) (Cg1) and the centroid of the 2-hydroxy-1-naphthaldehyde ring (C13-C18) (Cg2), with a Cg1 . . . Cg2 distance of 3.915 Å. The second interaction occurs at a distance of 3.594 Å, between Cg1 and the centroid Cg3 (C15/C16/C19/C20/C21/C22). The third interaction is between Cg4 (C1/C2/C6/C7/C8/C9) and Cg3, with the ring centroids separated by 3.653 Å (Figure 4b).

3.3. FT-IR and UV-Visible Absorption Spectra

Figure 5a shows the FT-IR spectra of the two complexes. Overall, both complexes show similar IR bands. The strong absorptions at 1604 cm⁻¹ and 1119 cm⁻¹, correspond to the C=O and C-O bonds of the aldehyde, respectively. The C-1 complex exhibits a broad band in the region of 3100–2800 cm⁻¹, which is attributed to the ν (C-H) of the aromatic ring. The bands appearing at 1562 cm⁻¹ and 1014 cm⁻¹ are due to the ν (C=N) and ν (C-N) of the 2,2'-bipyridine, respectively. The ν (C=N) band of the thieno ligand is observed at 2063 cm⁻¹. In the FT-IR spectrum of C-2, the bands appearing at 3100 cm⁻¹ and 2855 cm⁻¹ correspond to the aromatic ν (C-H). The spectrum also shows bands at 1434, 1274, and 730 cm⁻¹, which are assigned to the coordinated phenanthroline molecule [31,32].

The two complexes exhibit a d–d transition band at 624–640 cm⁻¹, and a band at 821–833 cm⁻¹, which is typical for square pyramidal geometry [30].

Figure 5b shows the UV-visible spectra in the range of 280–440 nm for C-1 and C-2. The absorption peaks of these two complexes are very similar. Nevertheless, those of C-2 are very weak. In the UV region, the two complexes show peaks near 290–300 nm due to the $\pi \rightarrow \pi^*$ aromatic ring. Moreover, we noticed two intense peaks, or a shoulder, in

the (305 → 315 nm) (I)—(310 → 325 nm) (II) region, which can be assigned to the charge transfer between the ligand and the metal.

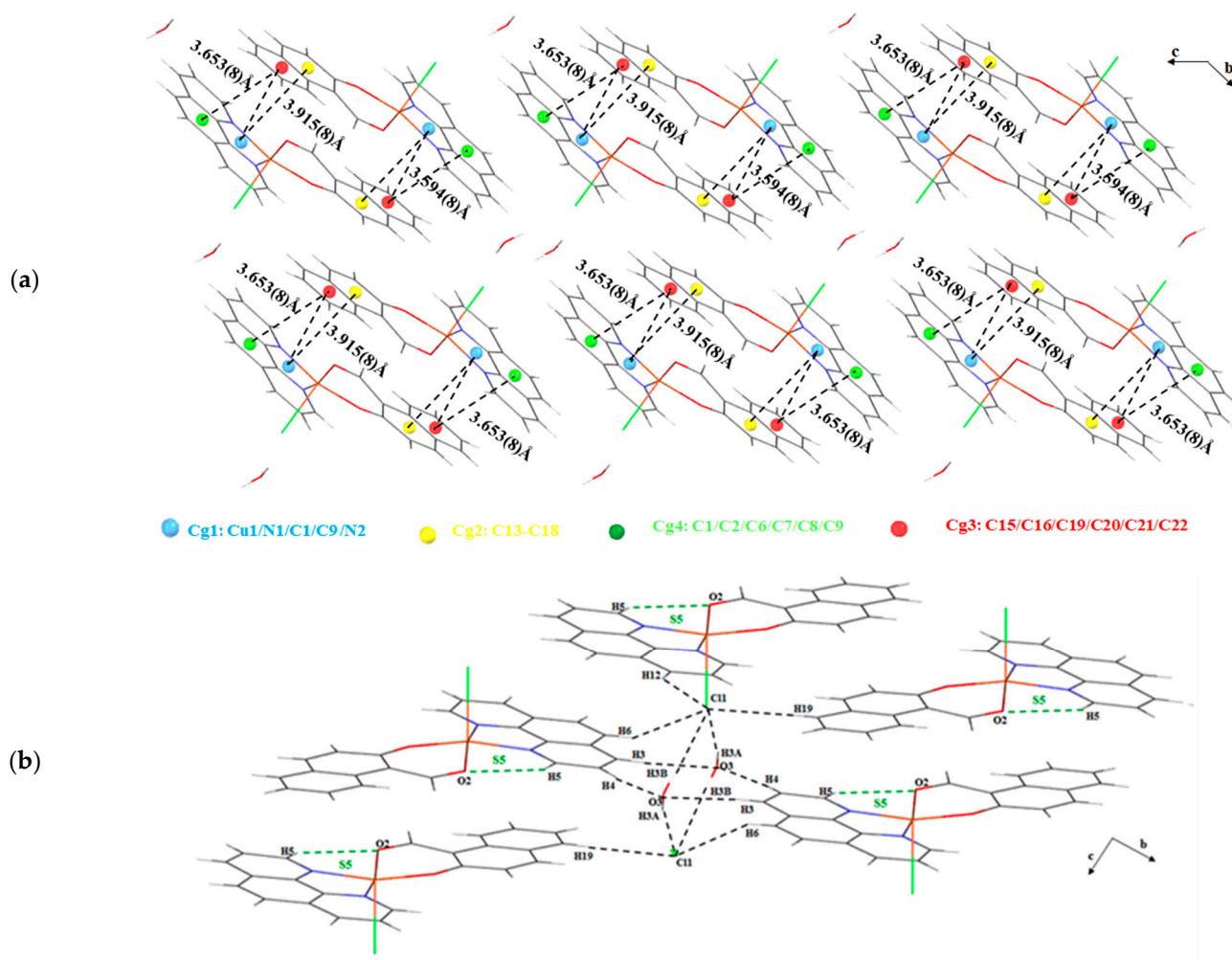


Figure 4. (a) Diagram packing of hydrogen bonding, parallel to (b,c). Dashed lines (green, black) indicate intra- and intermolecular H-bonds, respectively. (b) A view of the aromatic ring organization, with centroid-centroid distances (Å) for C-2.

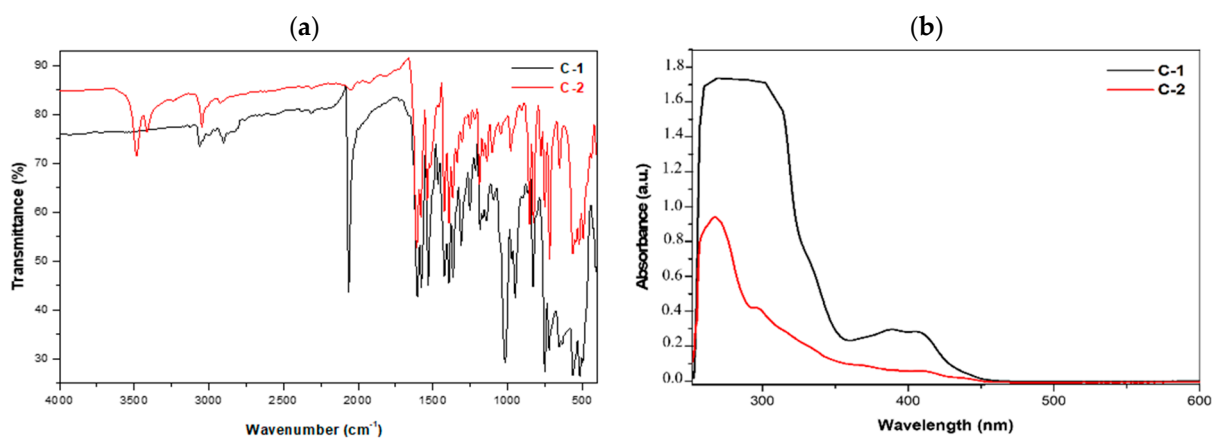


Figure 5. The FT-IR Spectrum (a) and the overlapping UV-visible spectrum in the DMSO (b) of complexes C-1 and C-2.

No d–d bands were observed in the spectra of the two complexes. These bands should be observed in the region of 500–600 nm. Their absence is due to the low concentration (10^{-5} mol·L⁻¹) of the solutions of the complexes.

3.4. Hirshfeld Surface Analysis

The intermolecular interactions and the packing modes that occur in crystalline structures can be studied quantitatively using Hirshfeld surface analysis [33]. Hirshfeld surfaces (HS) and fingerprint plots [34] were carried out using Crystal Explorer software [35].

The HS of the C-1 complex was mapped over d_{norm} in the range of -0.1832 to $+1.3833$ a.u., as shown in Figure 6a. Color coding is used for each specific region to identify the nature of the occurring intermolecular interactions, wherein contacts that are shorter, equal to, and longer than the sum of the van der Waals radii, correspond to the red, white and blue areas, respectively. The major interactions are caused by H···H, H···S/S···H, H···C/C···H, C···C and H···N/N···H contact. (Figure 6a).

The shape–index surface (Figure 6b) indicates the presence of blue and red triangles that are characteristic of π ··· π interactions between neighboring molecules, whereas the flat surface patches in the curvedness plots (Figure 6c) reveal planar stacking.

The 2-D fingerprint plots for the C-1 complex show the relative contributions of H···H, H···S/S···H, H···C/C···H, C···C and H···N/N···H contacts to the Hirshfeld surface; these are illustrated in Figure 6d. Contact between H···H comprise the predominant form of interactions (33.7%).

The HS of the C-2 complex is depicted in Figure 7a. The dominant interactions between (water) O-H, C-H, and Cl atoms are represented by the bright-red areas, which are marked as 1, 2, and 3. The light-red spots denoted as 4, 5, 6 and 7 are due to C-H···O and C-H···Cl interactions.

The π ··· π interactions in the C-2 complex are revealed by the characteristic blue and red triangles on the shape–index surface (Figure 7b), whereas planar stacking is identified by the curvedness plots (Figure 7c) that exhibit characteristic flat surface patches.

The relative contributions of the H···H, H···C/C···H, H···O/O···H, H···Cl/Cl···H and H···N/N···H contacts to the Hirshfeld surface in the C-2 complex are determined using the 2-D fingerprint plots, as illustrated in Figure 7d. As in the C-1 complex, the fingerprint plots of the C-2 complex show that the H···H contacts provide the most significant contribution to the Hirshfeld surface (45.1%).

3.5. Inhibitory Activity of the C-1 and C-2 Complexes against the HIV-1 Protease Enzyme

To provide insight into the binding mode of C-1 and C-2, a molecular docking investigation was carried out. As shown in Figure 8 (upper panel), the tested complexes occupied a common cavity in the receptor, suggesting that C-1 and C-2 block access to the active site of the HIV-1 protease. They are located in the hydrophobic pocket of HIV-1 protease, and they are surrounded by the Val32, Pro81, and Pro79 residues of the active site, and Gly48, Gly49, Ile50, Ile84, Ile47, and Leu84 of the subsites S1/S1', S2/S2', and S3/S3', wherein a strong hydrophobic interaction was observed, as illustrated in Figure 8 (lower panel). The ligand–receptor complex indicates that most of the ligand is positioned in the flap region of the enzyme, as represented by the Ile50, Gly51, Gly52, and Gly49 residues. No hydrogen bonds were found in the docked structures.

The estimated binding energies were -7.6 kcal/mol for C-1 and -7.1 kcal/mol for complex-ref, respectively. This result suggests that the tested compounds that were produced with HIV-1 protease formed stable complexes. The best ligand/receptor complex was formed by using C-2 with a binding energy equal to -8.3 kcal/mol.

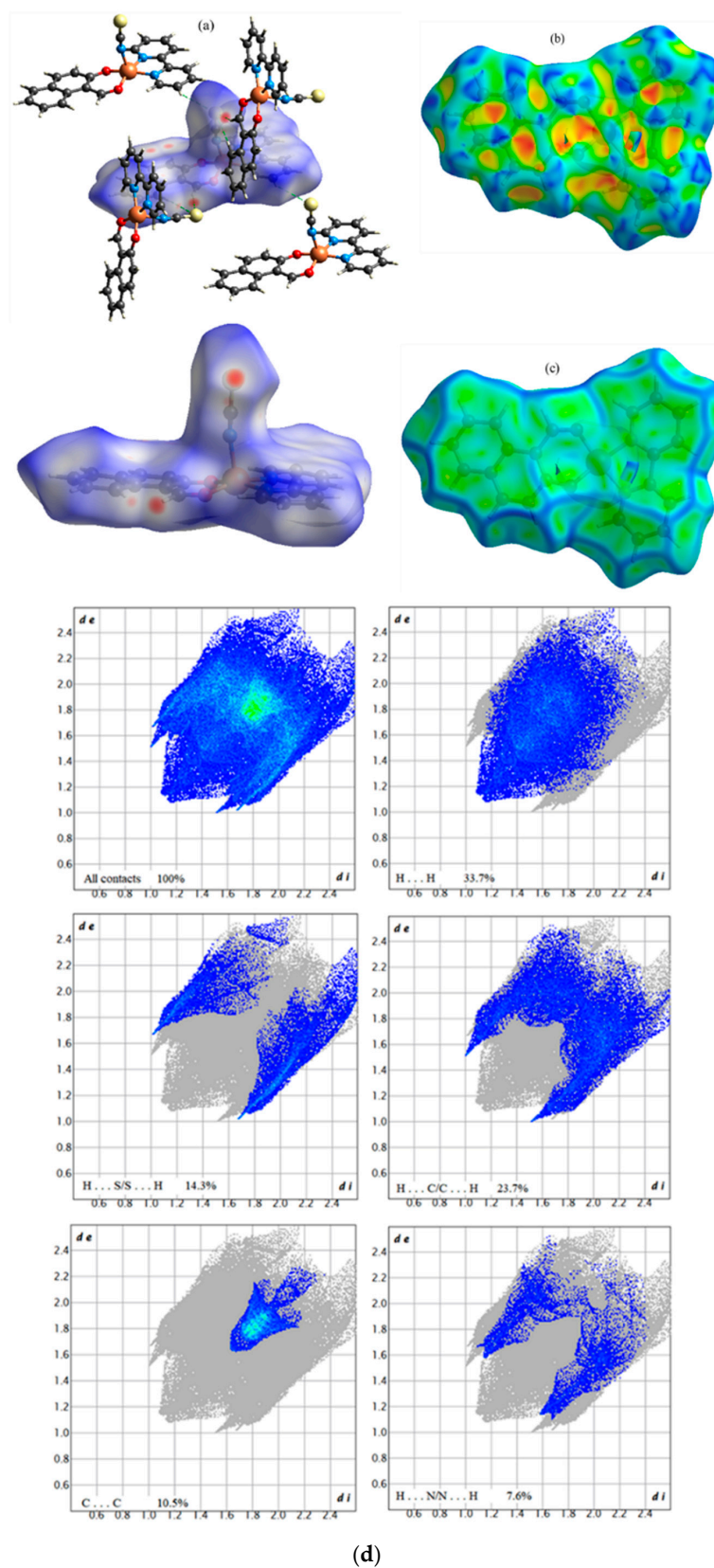


Figure 6. A view of the Hirshfeld surface for (I), which is mapped over (a) d_{norm} in the range of -0.1832 to $+1.3833$ arbitrary units. (b) Shape-index, (c) curvedness, and (d) 2-D fingerprint plots for the C-1 complex, which reveal the contributions of all contacts.

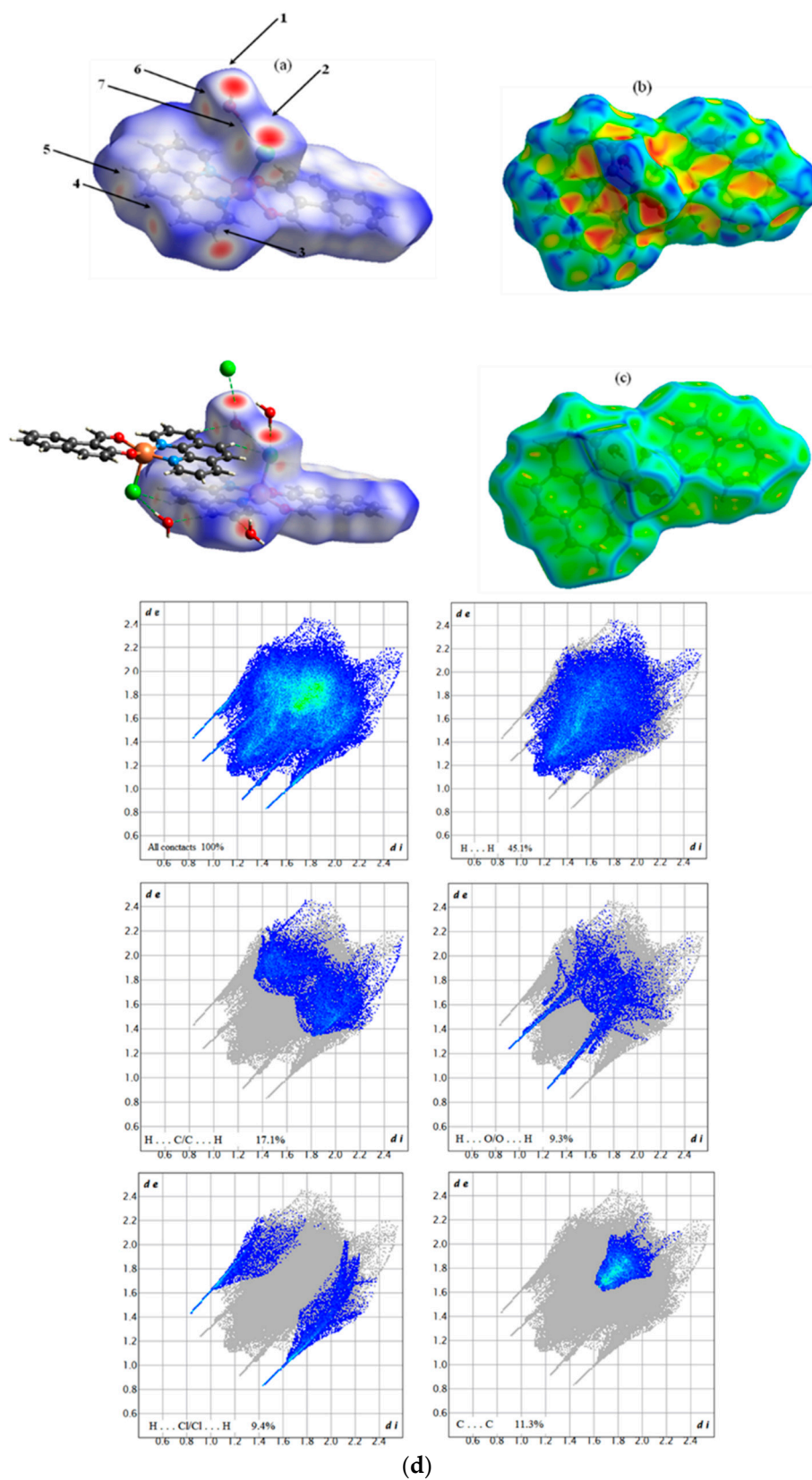


Figure 7. A view of the Hirshfeld surface for (II), which is mapped over (a) d_{norm} in the range of -0.4175 to $+1.3253$ arbitrary units. (b) Shape-index, (c) curvedness, and (d) 2-D fingerprint plots for the C-2 complex, which reveal the contributions of all contacts.

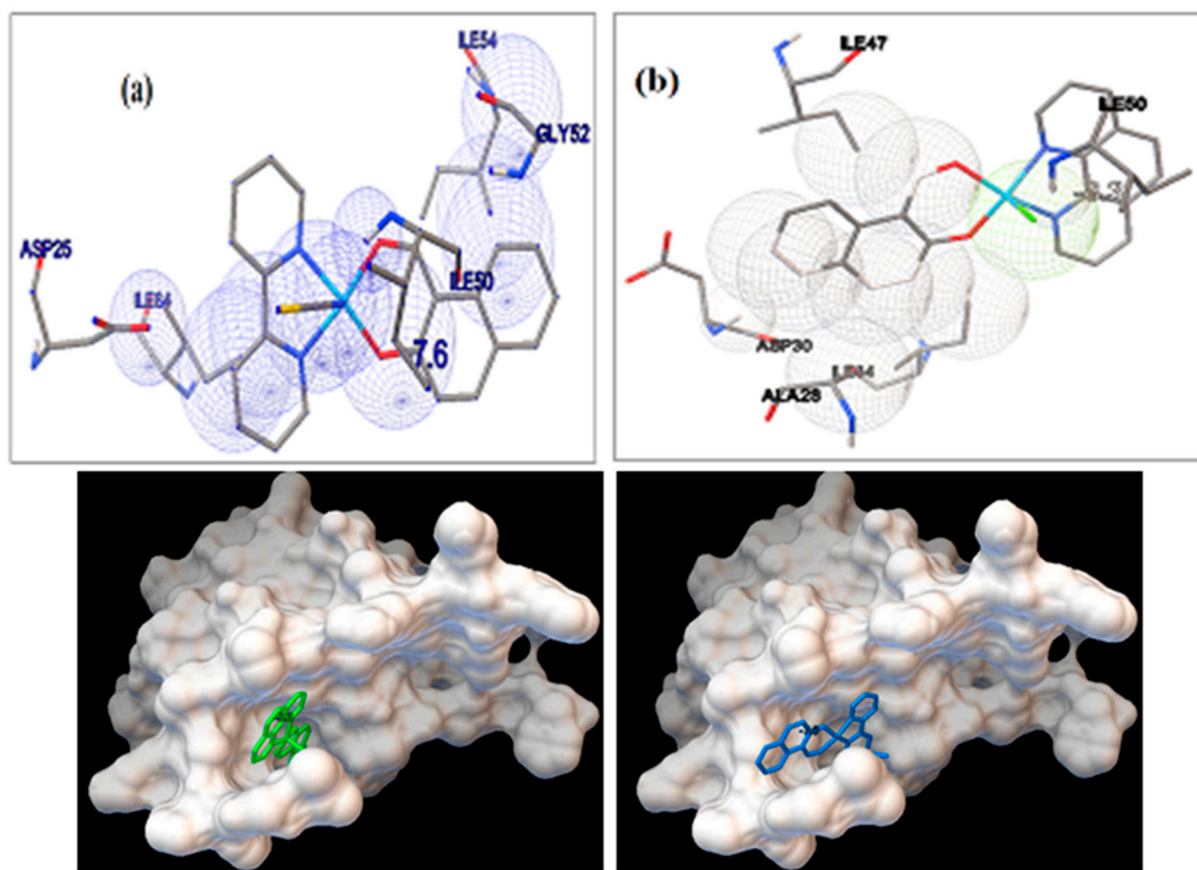


Figure 8. The upper panel shows the molecular docked model of C-1 (blue color) and C-2 (green color) in the HIV-1 protease active pocket. The enzyme is shown as a surface; the lower panel shows the best-docked conformation of C-1 (a) and C-2 (b) in the binding site of HIV-1.

4. Conclusions

Two new copper (II) complexes, based on 2,2'-bipyridine and 1,10-phenanthroline ligands, were synthesized and characterized using X-ray crystal diffraction, FT-IR, and UV-visible spectroscopies, as well as DFT calculations.

The crystalline structure of synthesized complexes consists of five coordinated Cu (II) ions in a square-pyramidal geometric structure, wherein the packing arrangement is mainly stabilized using hydrogen bonding networks and π - π stacking interactions. Hirshfeld surface analysis indicates that H \cdots H interactions account for 33.7% and 45.1% of the total Hirshfeld surface of the C-1 and C-2 complexes, respectively.

Based on computational results, the docking analysis revealed that both C-1 and C-2 Cu (II) complexes were more potent than the inhibitor reference when binding to the HIV-1 protease; the interactions that occurred were hydrophobic, resulting in their stabilization in the enzyme cavity.

Supplementary Materials: The following supporting information can be downloaded at: <https://www.mdpi.com/article/10.3390/cryst12081066/s1>, Figure S1: The copper square-pyramidal environment (a), and the dihedral angle between the two ligands (b) of C-2; Table S1: Selected experimental and calculated bond lengths (Å) and angles (°) for C-1; Table S2: Selected experimental and calculated bond lengths (Å) and angles (°) for C-2.

Author Contributions: Conceptualization, M.H. and H.M.; Data curation, M.H., I.H., M.D. and S.R.; Formal analysis, M.H., I.H., M.D. and S.R.; Funding acquisition, F.A.M.A., M.A.A. and S.T.; Investigation, M.H. and I.H.; Methodology, M.D., Y.B. and S.R.; Project administration, H.M.; Resources, I.H., M.D. and H.M.; Software, M.H. and M.D.; Supervision, H.M.; Validation, F.A.M.A., M.A.A., S.T. and H.M.; Writing—original draft, M.H., I.H., M.D. and Y.B.; Writing—review & editing,

Y.B., N.S., F.A.M.A., M.A.A. and S.T. All authors have read and agreed to the published version of the manuscript.

Funding: This research received no external funding.

Institutional Review Board Statement: Not applicable.

Informed Consent Statement: Not applicable.

Data Availability Statement: The data presented in this study are available on request from the corresponding author.

Conflicts of Interest: The authors declare no conflict of interest.

References

1. Janzen, D.E.; Wang, X.; Carr, P.W.; Mann, K.R. Synthesis and characterization of three geometric isomers of ruthenium(II)(2,2'-bipyridyl) (salicylaldehyde) 2. *Inorg. Chim. Acta* **2004**, *357*, 3317–3324. [[CrossRef](#)]
2. Vigato, P.A.; Tamburini, S. The challenge of cyclic and acyclic schiff bases and related derivatives. *Coord. Chem. Rev.* **2004**, *248*, 1717–2128. [[CrossRef](#)]
3. Yamada, S. Advancement in stereochemical aspects of Schiff base metal complexes. *Coord. Chem. Rev.* **1999**, *190*, 537–555. [[CrossRef](#)]
4. Jayamani, A.; Bellam, R.; Gopu, G.; Ojwach, S.O.; Sengottuvelan, N. Copper(II) complexes of bidentate mixed ligands as artificial nucleases: Synthesis, crystal structure, characterization and evaluation of biological properties. *Polyhedron* **2018**, *156*, 138–149. [[CrossRef](#)]
5. Elmali, A.; Elerman, Y. Crystal structure of (2,2'-Dipyridyl)-(2-hydroxynaphthaldehydato) copper (II) perchlorate. *Anal. Sci.* **2002**, *18*, 855–856. [[CrossRef](#)] [[PubMed](#)]
6. Seco, J.M.; Gonzalez Garmendia, M.J.; Quiros, M. Synthesis characterization of tris (2,2'-bipyridine) and tris (1,10-phenanthroline) copper (II) hexafluorophosphate. Crystal structure of the phenanthroline complex. *J. Coord. Chem.* **2002**, *55*, 345–351. [[CrossRef](#)]
7. Adelaide, O.M.; Abidemi, O.O.; Olubunmi, A.D. Synthesis, characterization and antibacterial studies of some copper (II) complexes of 2,2'-bipyridine and 1.10-phenanthroline. *J. Chem. Pharm. Res.* **2013**, *5*, 69–73.
8. Agwaral, M.O.; Ndifon, P.T.; Ndosiril, N.B.; Paboudam, A.G.; Yufanyi, D.M.; Mohamadou, A. Synthesis, Characterisation and Antimicrobial activities of Cobalt (II), Copper (II) and Zinc (II) mixed-ligand complexes containing 1,10 Phenanthroline and 2,2-Bipyridine. *Bull. Chem. Soc. Ethiop.* **2010**, *24*, 383–389.
9. Lobana, T.S.; Indoria, S.; Jassal, A.K.; Kaur, H.; Arora, D.S.; Jasinski, J.P. Synthesis, structures, spectroscopy and anti-microbial properties of complexes of Copper(II) with salicylaldehyde N-substituted thiosemicarbazones and 2,20-bipyridine or 1,10-phenanthroline. *Eur. J. Med. Chem.* **2014**, *76*, 145–154. [[CrossRef](#)]
10. Sierra-Aragón, S.; Walter, H. Targets for Inhibition of HIV Replication: Entry, Enzyme Action, Release and Maturation. *Intervirology* **2012**, *55*, 84–97. [[CrossRef](#)]
11. Ghosh, A.K.; Osswald, H.L.; Prato, G. Recent Progress in the Development of HIV-1 Protease Inhibitors for the Treatment of HIV/AIDS. *J. Med. Chem.* **2016**, *59*, 5172–5208. [[CrossRef](#)]
12. Wang, Y.; Lv, Z.; Chu, Y. HIV protease inhibitors: A review of molecular selectivity and toxicity. *HIV/AIDS-Res. Palliat. Care* **2015**, *7*, 95–104. [[CrossRef](#)]
13. Lee, C.; Yang, W.; Parr, R.G. Development of the Colic-Salvetti correlation-energy formula into a functional of the electron density. *Phys. Rev. B* **1988**, *37*, 785. [[CrossRef](#)]
14. Becke, A.D. Density-functional thermochemistry. I. The effect of the exchange-only gradient correction. *J. Chem. Phys.* **1992**, *96*, 2155–2160. [[CrossRef](#)]
15. Becke, A.D. Density-functional thermochemistry. III. The role of exact exchange. *J. Chem. Phys.* **1993**, *98*, 5648–5652. [[CrossRef](#)]
16. Becke, A.D. A new mixing of Hartree-Fock and local density-functional theories. *J. Chem. Phys.* **1993**, *98*, 1372–1377. [[CrossRef](#)]
17. Trott, O.; Olson, A.J. AutoDock Vina: Improving the speed and accuracy of docking with a new scoring function, efficient optimization and multithreading. *J. Comp. Chem.* **2010**, *31*, 455–461. [[CrossRef](#)]
18. Lebon, F.; Ledecq, M.; Benatallah, Z.; Sicsic, S.; Lapouyade, R.; Kahn, O.; Garçon, A.; Reboud-Ravaux, M.; Durant, F. Synthesis and structural analysis of copper(II) pyridine amide complexes as HIV-1 protease inhibitors. *J. Chem. Soc. Perkin Trans.* **1999**, *2*, 795–800. [[CrossRef](#)]
19. Mager, P.P. The active site of HIV-1 protease. *Med. Res. Rev.* **2001**, *21*, 348–353. [[CrossRef](#)]
20. Mudgal, M.M.; Birudukota, N.; Doke, M.A. Applications of Click Chemistry in the Development of HIV Protease Inhibitors. *Inter. J. Med. Chem.* **2018**, *2018*, 2946730.
21. Bruker. *APEX2 and SAINT*; Bruker AXS Inc.: Madison, WI, USA, 2011.
22. Sheldrick, G.M. A short history of SHELX. *Acta Crystallogr. Sect. A* **2008**, *A64*, 112–122. [[CrossRef](#)]
23. Frisch, M.J.; Trucks, G.W.; Schlegel, H.B.; Scuseria, G.E.; Robb, M.A.; Cheeseman, J.R.; Scalmani, G.; Barone, V.; Men-nucci, B.; Petersson, G.A.; et al. *Gaussian 09, Revision B.01*; Gaussian, Inc.: Wallingford, CT, USA, 2010.

24. O'Boyle, N.M.; Banck, M.; James, C.A.; Morley, C.; Vandermeersch, T.; Hutchison, G.R. Open babel: An open chemical toolbox. *J. Cheminform.* **2011**, *3*, 33. [[CrossRef](#)]
25. The Open Babel Package, Version 2.3.1. Available online: <http://openbabel.org> (accessed on 30 March 2022).
26. Addison, A.W.; Rao, T.N.; Reedijk, J.; van Rijn, J.; Verschoor, G.C. Synthesis, structure, and spectroscopic properties of copper(II) compounds containing nitrogen–sulphur donor ligands; the crystal and molecular structure of aq-ua[1,7-bis(N-methylbenzimidazol-2'-yl)-2,6-dithiaheptane]copper(II) pe. *J. Chem. Soc. Dalt. Trans.* **1984**, *7*, 1349–1356. [[CrossRef](#)]
27. Asgharpour, Z.; Farzaneh, F.; Abbasi, A. Synthesis, characterization and immobilization of a new cobalt(ii) complex on modified magnetic nanoparticles as catalyst for epoxidation of alkenes and oxidation of activated alkanes. *RSC Adv.* **2016**, *6*, 95729–95739. [[CrossRef](#)]
28. Bernstein, J.; Davis, R.E.; Shimoni, L.; Chang, N.-L. Patterns in Hydrogen Bonding: Functionality and Graph Set Analysis in Crystals. *Angew. Chem. Int. Ed. Engl.* **1995**, *34*, 1555–1573. [[CrossRef](#)]
29. Etter, M.C.; Macdonald, J.C.; Bernstein, J. Graph-set analysis of hydrogen-bond patterns in organic crystals. *Acta Crystallogr. Sect. B Struct. Sci.* **1990**, *46*, 256–262. [[CrossRef](#)] [[PubMed](#)]
30. Hangan, A.; Bodoki, A.; Oprean, L.; Alzuet, G.; Liu-Gonzalez, M.; Borrás, J. Synthesis, crystallographic, spectroscopic characterization and magnetic properties of dimer and monomer ternary copper(II) complexes with sulfonamide derivatives and 1,10-phenanthroline. Nuclease activity by the oxidative mechanism. *Polyhedron* **2010**, *29*, 1305–1313. [[CrossRef](#)]
31. Lara, J.G.; Sanchez, A.A. The infra-red spectra of 2-hydroxy-1-naphthaldehyde complexes. *Spectrochim. Acta Part A* **1967**, *23*, 1299–1306. [[CrossRef](#)]
32. Mohapatra, R.K.; Saikishore, V.P.; Azam, M.; Biswal, S.K. Synthesis and physicochemical studies of a series of mixed-ligand transition metal complexes and their molecular docking investigations against Coronavirus main protease. *Open Chem.* **2020**, *18*, 1495–1506. [[CrossRef](#)]
33. Spackman, M.A.; Jayatilaka, D. Hirshfeld surface analysis. *CrystEngComm* **2009**, *11*, 19–32. [[CrossRef](#)]
34. Spackman, M.A.; McKinnon, J.J. Fingerprinting intermolecular interactions in molecular crystals. *CrystEngComm* **2002**, *4*, 378–392. [[CrossRef](#)]
35. Turner, M.J.; McKinnon, J.J.; Wolff, S.K.; Grimwood, D.J.; Spackman, P.R.; Jayatilaka, D.; Spackman, M.A. *Crystal Explorer 17.5*; The University of Western Australia: Perth, Australia, 2017.